

GT2011-4* (- %

TURBULENCE AND HEAT TRANSFER MEASUREMENTS IN AN INCLINED LARGE SCALE FILM COOLING ARRAY – PART I, VELOCITY AND TURBULENCE MEASUREMENTS

Lamyaa A. El-Gabry

Mechanical Engineering Department
The American University in Cairo
New Cairo, Egypt

Douglas R. Thurman

US Army Research Laboratory
Glenn Research Center
Cleveland, Ohio, USA

Philip E. Poinsette, James D. Heidmann

Turbomachinery and Heat Transfer Branch
NASA Glenn Research Center
Cleveland, Ohio, USA

ABSTRACT

A large-scale model of an inclined row of film cooling holes is used to obtain detailed surface and flow field measurements that will enable future computational fluid dynamics code development and validation. The model consists of three holes of 1.9-cm diameter that are spaced 3 hole diameters apart and inclined 30° from the surface. The length to diameter ratio of the coolant holes is about 18. Measurements include film effectiveness using IR thermography and near wall thermocouples, heat transfer using liquid crystal thermography, flow field temperatures using a thermocouple, and velocity and turbulence quantities using hotwire anemometry. Results are obtained for blowing ratios of up to 2 in order to capture severe conditions in which the jet is lifted. This first part of the two-part paper presents the detailed velocity component and turbulence stresses along the centerline of the film-cooling hole and at various streamwise locations.

INTRODUCTION

Film cooling is a critical aspect of hot gas path component design; without which it would be impossible for parts to survive the gas temperatures that exceed operable limits of the latest in material and coating technology. The importance of cooling and film cooling in particular has been

the motivation of a vast body of research on the topic and thousands of papers and articles on the subject.

Goldstein [1] reviewed 25 years of early analytical and experimental research on flat plate geometries. The effect of injection angle, blowing ratio, density ratio, and momentum ratio were investigated for a circular film-cooling hole. Thole et al [2] varied mass, velocity, and density ratio for a row of inclined jets and measured the flow temperatures along the film centerline and at various streamwise locations; results show that the thermal field characteristics can be best scaled using the ratio of coolant to freestream momentum flux. At low momentum flux, the cooling jet remains attached upon ejection. At moderate momentum flux ratios, the film starts out detached at the hole exit and then reattaches to the surface. At higher yet momentum flux, the film exits the hole detached and remains detached from the surface. Sinha et al [3] studied the effects of the same parameters on film cooling effectiveness using surface mounted thermocouples along the jet centerline and at spanwise locations. It is interesting to note that unlike the temperature field, which scales with momentum ratio, the film effectiveness for detached jets does not appear to scale with any parameter. For attached jets, however, effectiveness scaled with mass flux ratio.

Injection angle is an important parameter in controlling the jet detachment in addition to momentum

ratio. Foster et al [4] studied the effect of injection angle (35, 55, and 90-degree incline) on flow velocities and film effectiveness using a Pitot tube for mapping streamwise velocities at a blowing ratio of 1.4. Later, Kohli et al [5] used Laser Doppler Velocimetry to study the effect of injection angle (55 and 35 deg incline) at a fixed density ratio of 1.6 on the velocity fields and also presented results on the thermal field and adiabatic effectiveness for the different injection angles.

The density ratio of the coolant to mainstream flow accounts for density differences in turbine engine conditions where the coolant is at a significantly lower temperature than the hot gas and therefore at a higher density. Under lab conditions, the simplest density ratio to evaluate is unity, which is not representative of engine conditions. To achieve higher density ratios, one can cryogenically cool the coolant stream or use a denser gas than air for the coolant. The effect of density ratio has been studied extensively [6-9]. Foster et al [6] used a mass transfer analogy and reports streamwise variation of film effectiveness at the hole centerline to study the effect of velocity and density ratio. Pietrzyk et al [7-9] studied the hydrodynamics of film cooling for an array of 35-degree inclined holes (spacing of 3D and length of 3.5D) at a blowing ratio of 0.5 using LDV measurements to measure the velocities and turbulence field at a density ratio of 2 [7] and a density ratio of 1 [8].

Despite the wealth of knowledge that already exists on the subject of film cooling flows, the modeling and prediction of such flows continues to present a challenge [10, 11] and the gas turbine heat transfer design community continues to rely on empiricism for “conventional” designs and perhaps some CFD for detailed design or evaluation non-conventional concepts. Complex CFD models requiring weeks to run are still out of reach for the mainstream design community. Therefore, there is motivation to “model” turbulence and other physics because that is what offers reasonable turnaround time for analyses today. The intent of the research is to obtain data that would enable the development of numerical models and the validation of CFD codes. This includes detailed results on the velocity components and turbulence stresses, particularly at difficult to predict conditions of high blowing. Although there exist test data on turbulence and velocity in the open literature [e.g. 5, 7, 9, 12, 13] it is limited in one way or another. Either data is limited to hydrodynamics only or surface results only or the blowing ratio is low meaning that the film is fully attached and therefore not the most challenging case for numerical predictions. Andreaopolous et al [12] measured mean and turbulent velocity components using a triple-wire probe for a 90-degree jet injection (less relevant for film cooling) and showed that the turbulent kinetic energy and turbulent stresses were closely related to the mean velocity gradient. Kohli et al [13] look at the momentum terms but also made simultaneous velocity and temperature

measurements to look at turbulent transport of heat and momentum; however, the momentum ratio for that case is 0.16 and the blowing ratio is 0.4 which produces a film that is fully attached and relatively easier to predict.

To obtain measurements for validation, a large-scale test facility is needed in order to obtain the spatial resolution to resolve the shear layers and wake region and other complex highly three-dimensional regimes associated with detached films. Various hotwire probes are used to obtain the three-dimensional velocity components and turbulent stresses along the centerline and at various streamwise planes. In addition, we report in a companion paper the thermal field and surface film effectiveness obtained from the same test rig at identical test conditions and locations as the velocity and turbulence measurements thereby offering a plethora of high resolution test data for CFD model development and validation.

NOMENCLATURE

D	diameter of film cooling hole
DR	jet to mainstream density ratio $= \rho_j / \rho_\infty$
I	jet to mainstream momentum flux ratio $= \rho_j U_j^2 / \rho_\infty U_\infty^2$
L	length of film cooling hole
M	blowing ratio $= \rho_j U_j / \rho_\infty U_\infty$
n	number of samples of hot wire velocity data (based on sampling frequency and time)
Re	Reynolds number based on hole diameter and inlet conditions
T_∞	mainstream inlet temperature
T_c	coolant temperature
U	velocity component in streamwise direction
U^*	normalized U-velocity $= U / U_\infty$
u'	fluctuations in streamwise velocity U
u^*	normalized rms U-velocity fluctuations $= \sqrt{\frac{\sum (u_{instantaneous_i} - u_{avg})^2}{n}}$
\overline{uv}	turbulent shear stress (x, y correlation)
$u'v'^*$	normalized shear stress $= \overline{uv} / U_\infty^2$
\overline{uw}	turbulent shear stress (x, z correlation)
$u'w'^*$	normalized shear stress $= \overline{uw} / U_\infty^2$
V	velocity component in spanwise direction
v'	fluctuations in spanwise velocity V
v^*	normalized rms U-velocity fluctuations $= \sqrt{\frac{\sum (v_{instantaneous_i} - v_{avg})^2}{n}}$
VR	jet to mainstream velocity ratio $= U_j / U_\infty$
W	velocity component in wall-normal direction
w'	fluctuations in wall-normal velocity W

w^* normalized rms U-velocity fluctuations

$$= \sqrt{\frac{\sum(w_{\text{instantaneous}_i} - w_{\text{avg}})^2}{n}}$$

X streamwise distance from hole leading edge

Y spanwise distance from hole centerline

Z vertical distance from tunnel floor (flat plate surface)

ρ density (average)

Subscripts

avg average

rms root mean square

∞ freestream (or mainstream)



Fig 2. Photograph of test model

EXPERIMENTAL APPARATUS AND PROCEDURES

The apparatus, shown in Figure 1, consists of an open-loop wind tunnel with a temperature-controlled coolant loop. The tunnel is a suction type tunnel that draws air from the room and passes it through screens, grid and filters prior to entering the test section. The freestream velocity is 9.1 m/s (30 ft/sec) and the Reynolds number based on freestream velocity and coolant hole diameter is 11,000. The test section is a square section 20.32x20.32-cm (8x8-inch) and 86.36 cm (34 inch) in length. The freestream turbulence intensity at the inlet of the test section is about 4%.

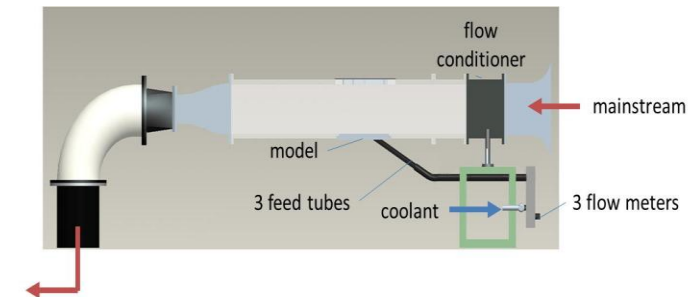


Fig 1. Wind tunnel test apparatus

The film-cooling model (Figures 2 and 3) is a large-scale (~ 30X) model to enable high spatial resolution near the film coolant hole. It consists of a three-hole array of film cooling holes that are fed by three long tubes. The model is inserted into the test section of the tunnel such that the heat transfer surface forms the wind tunnel floor. The cooling holes have a diameter $D = 1.9$ cm (0.75 inch), spacing $Y/D=3$, and are angled 30 degrees from the streamwise direction. The coolant was fed through a manifold to three separate flow meters, then through 45 cm of hose and 30 cm of acrylic tube, in an attempt to generate fully developed flow at the hole exit. The coolant flow path from flow meter to hole exit was nearly twice the required entrance length ($L/D > 23$ for the high blowing ratio case) for turbulent flow. The entire coolant path was insulated.

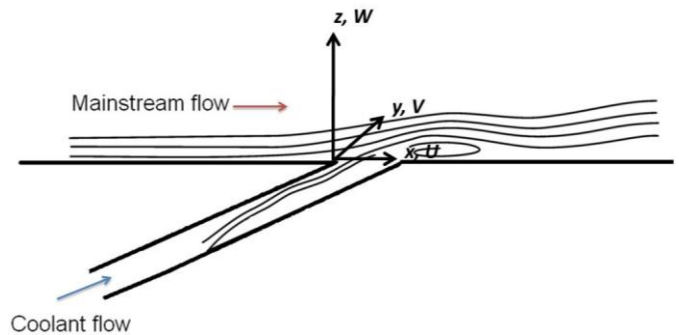


Fig 3. Schematic of film cooling model

For the thermal tests [14], the coolant is chilled 30-40°F below the freestream temperature; however, for the hotwire measurements presented here, the coolant and freestream are maintained at ambient temperature. Measurements are obtained for a density ratio $DR \sim 1$, velocity ratio $VR = 1$ to 2, blowing ratio $M = 1$ to 2, and consequently a momentum flux ratio $I = 1$ to 4, nominally.

Instrumentation. A Pitot tube is used to measure the freestream velocity at the inlet of the wind tunnel. Thermocouples are used to measure coolant and freestream temperatures. Velocity and turbulence are measured using a single wire and a two-wire hotwire system for obtaining components. The hotwire is powered by a constant temperature anemometry system and data is acquired at a rate of 50 kHz for 3 seconds.

The hotwire is calibrated in-situ in the wind tunnel test section with the coolant flow turned off and the wire positioned normal to the flow direction. The tunnel velocity is varied between 0 to 45.7 m/s (150 ft/s) and the voltage across the wire is recorded and correlated to the measured velocity using a fourth-order polynomial.

For the two-wire (aka cross-wire, X-wire) probes, a similar procedure is followed. Two different X-wire probes are used; one is used to measure U- and V-components of velocity and the other is used to measure U-

and W-components. In both cases, the two wires are separated by some distance and crossed to make an “X” shape. To calibrate the X-probe, the probe is positioned in the wind tunnel such that the wires are at a 45° to the mainstream flow direction; the coolant flow turned off and the tunnel velocity is varied across the same range 0 to 45.7 m/s (150 ft/s). The voltage for both wires is recorded and correlated to the velocity as measured by the Pitot tube. Since the wires are at a known angle to the flow, it is possible using trigonometric relations to deduce the two components of velocity.

The uncertainty in the velocity fluctuations and Reynolds stresses depends on several factors, such as probe type, calibration, orientation, flow angles, etc. [15][16] The measurement uncertainty for these experiments was calculated to be less than 4% for mean velocities and 5% for fluctuations. The Reynolds stress uncertainties were typically less than 15% but were as much as 25% in some of the high turbulence regions.

EXPERIMENTAL RESULTS AND DISCUSSION

The three components of velocity are measured and several (but not all) turbulent stresses are measured. Equations 1 and 2 are the Reynolds Averaged Navier Stokes equations obtained by substituting the Reynolds decomposition into the governing equations of mass and momentum, respectively, and ensemble averaging the result.

$$\frac{\partial \rho}{\partial t} + \frac{\partial \rho U_i}{\partial x_i} = 0 \quad [1]$$

$$\frac{\partial \rho U_i}{\partial t} + \frac{\partial \rho U_j U_i}{\partial x_j} = \frac{\partial}{\partial x_j} \left(\mu \frac{\partial U_i}{\partial x_j} - \rho \overline{u_j u_i} \right) - \frac{\partial P}{\partial x_i} + S_i \quad [2]$$

The turbulent stresses are the $\rho \overline{u_j u_i}$ terms in Equation 2. These six Reynolds stresses are generally “modeled” using various turbulence models. Some models are more simplistic than others and all models inherently make some assumptions. The intent of this paper is to measure the turbulent quantities as well as the velocity components at a large scale so as to provide results with the spatial resolution needed for numerical code and model development and validation.

The velocity and turbulence results are presented as contours along the jet centerline, at four streamwise locations for blowing ratio of 2, and at one streamwise location for blowing ratio of 1. Data was normalized, but slight inconsistencies may exist between the contours along the centerline and at the various streamwise locations due to data being taken on different days. No attempt was made to correct for differences in the measurement volumes of the two probes used in this study, but the differences in the U-component of velocity was generally within the measurement

uncertainty. Thus only the U-component from the L-probe (measuring the U and W components) will be presented. The detailed results are presented in a methodical manner that would facilitate other comparisons such as future numerical predictions evaluated for code validation. The turbulence quantities that are measured and reported are: the normalized root-mean square of the velocity fluctuations ($\frac{u'_{rms}}{U_\infty}$, $\frac{v'_{rms}}{U_\infty}$, and $\frac{w'_{rms}}{U_\infty}$) and the normalized shear stresses ($\frac{\overline{uv}}{U_\infty^2}$ and $\frac{\overline{uw}}{U_\infty^2}$).

Figure 4 shows the non-dimensional U-velocity contours along the jet centerline for a nominal blowing ratio of 2. The grid points show the measurement locations of the hotwire probe. The high velocity core extends 1.5 hole diameters from the wall. The jet is lifted from the surface and the wake region is at nearly freestream velocity suggesting that the mainstream wraps around the coolant jet and passes in the wake, similar to a cylinder in crossflow. Upstream of the jet injection, there is a region of lower velocity (down to 0.6 of the freestream) suggesting that the mainstream flow decelerates as it approaches the coolant jet.

Figure 5 shows the non-dimensional U-velocity contours for a nominal blowing ratio of 2 at four streamwise locations: roughly 2, 4, 6, and 8 hole diameters from the jet leading edge. Superimposed on the contours are velocity vectors obtained from the two different X-probes. The streamwise contours confirm that the jet is lifted from the surface. One also can see the kidney vortex imprint on the contours and the counter-rotating vortex pair.

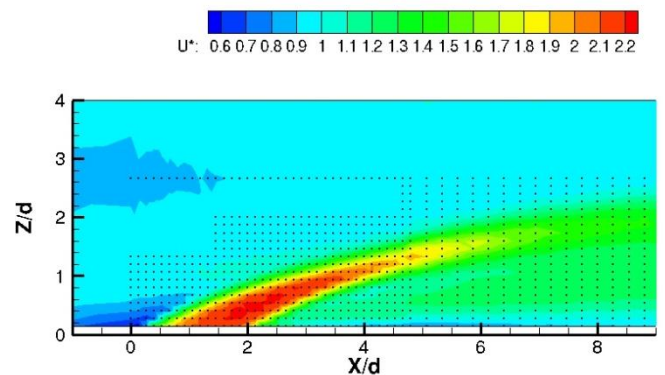


Fig 4. U-velocity contours along jet centerline at BR ~ 2; dots show measurement locations

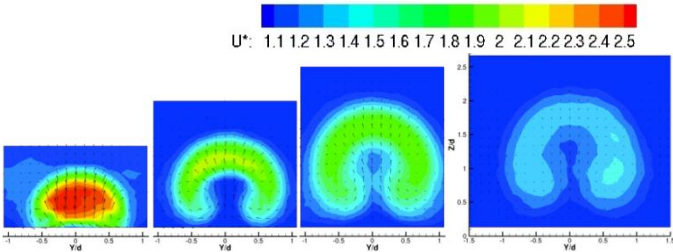


Fig 5. Velocity vectors and U-velocity contours at $X/d \sim 2, 4, 6,$ and 8 at $BR \sim 2$

Figure 6 shows the root mean square of the turbulent fluctuations of the U-velocity based on the standard deviation of the U-velocity signal from the L-probe crosswire. Figure 7 shows the same parameter at the four streamwise locations. Figure 6 suggests that the highest fluctuations up to and exceeding 25% of the freestream velocity are along the jet-freestream interface or shear layers. There is also elevated turbulence in the wake region of the jet but the highest levels are at the shear layers both upstream and downstream of the injection. Consistent with the centerline values, Figure 7 shows that there is a region of high intensity at the jet-freestream interface but there also appears to be moderately high turbulence in the wake of the jet.

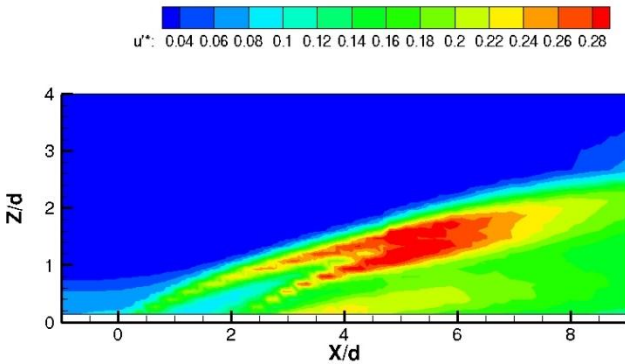


Fig 6. Turbulent fluctuations u' along jet centerline at $BR \sim 2$

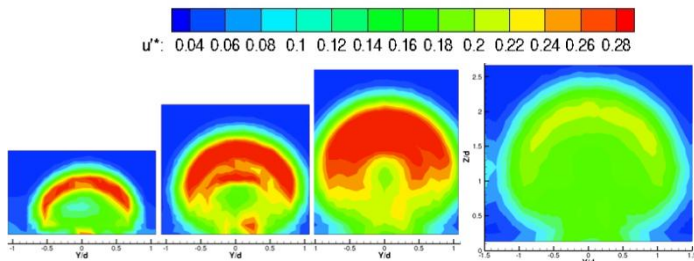


Fig 7. Turbulent fluctuations u' at $X/d \sim 2, 4, 6,$ and 8 at $BR \sim 2$

Figure 8 shows the turbulent fluctuations of the W-component (i.e. Z-component) of velocity based on the standard deviation of the W-velocity signal from the L-probe crosswire along the jet centerline for a nominal blowing ratio of 2. Figure 9 shows the same quantity at four streamwise planes. There are higher stresses in the shear layer and overall the intensity of the W-fluctuations is comparable to the U-fluctuations in Figures 6 and 7, though perhaps slightly lower. A difference that may be noteworthy is in the wake region around the centerline of the jet: in Figures 6 and 7, the U-component was elevated in this nearwall wake region (intensity in excess of 22%) whereas the W-component in Figures 8 and 9 is relatively lower near the wall (intensity of about 10%). This difference between the U- and W-components indicate that in the nearwall wake region, the turbulence is anisotropic and may explain the deficiency in turbulence models that assume isotropy.

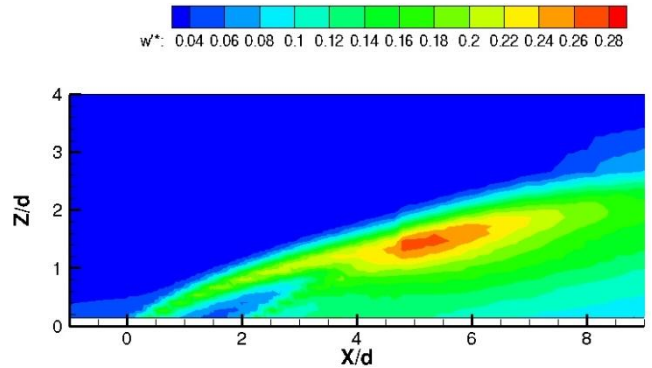


Fig 8. Turbulent fluctuations w' along jet centerline at $BR \sim 2$

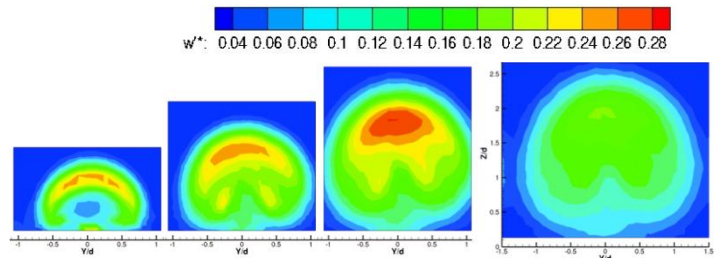


Fig 9. Turbulent fluctuations w' at $X/d \sim 2, 4, 6,$ and 8 at $BR \sim 2$

Due to symmetry the V-component of velocity along the jet centerline is negligible. The V-component is the hole-to-hole component of velocity. The fluctuations in the V-component are also small. Figure 10 shows the intensity of the fluctuations in V at the four streamwise locations.

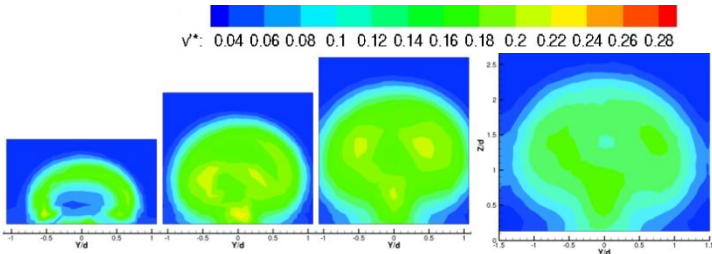


Fig 10. Turbulent fluctuations v' at $X/d \sim 2, 4, 6,$ and 8 at $BR \sim 2$

Up to this point, the results presented have been for the velocity components and the velocity fluctuations which are an indication of the turbulence intensity in the three directions. Figures 11 and 12 present the normalized shear stress \overline{uw}/U_∞^2 along the jet centerline and at the four streamwise locations while Figure 13 shows the \overline{uv}/U_∞^2 stress at the four streamwise locations. Unlike the turbulent fluctuations which have no direction (i.e. intensity only) the shear stresses can be either positive or negative. Figure 11 shows the highest magnitude to be at the shear layers between the jet and freestream; a positive correlation is along the freestream side of the jet and a negative one is on the downstream wake interface. The streamwise contours in Figure 11 also show the high stress region at the shear layer and at X/d of 4, it is possible to see both the positive and negative regions. Figure 13 shows the turbulent shear stress \overline{uv}/U_∞^2 to be roughly of the same order of magnitude as \overline{uw}/U_∞^2 . It is unclear why the stress is always positive and somewhat unsymmetrical about the centerline, but could be due to a small flow disturbance.

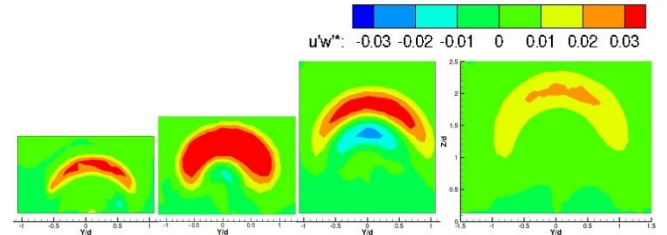


Fig 12. Turbulent stress \overline{uw}/U_∞^2 at $X/d \sim 2, 4, 6,$ and 8 at $BR \sim 2$

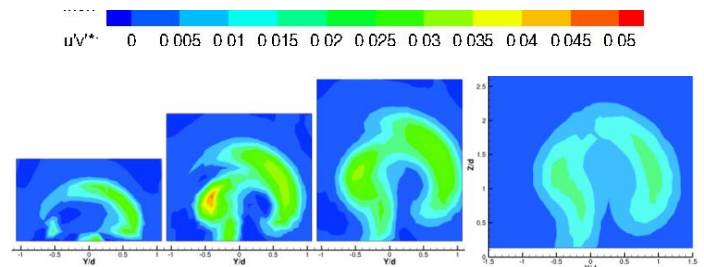


Fig 13. Turbulent stress \overline{uv}/U_∞^2 at $X/d \sim 2, 4, 6,$ and 8 at $BR \sim 2$

Figures 14 through 23 focus on the lower blowing ratio case and offer velocity and turbulence results at a nominal blowing ratio of 1. The results for this case are shown at centerline and at the streamwise location X/d of 4.

The velocity contours in Figure 14 show a stronger deflection of the jet; however the film still does not appear completely attached at this blowing ratio. The core extends slightly less than one hole diameter from the wall and as with the high blowing ratio case, it appears that the freestream decelerates as it approaches the jet to a value that is 0.6 of the freestream velocity.

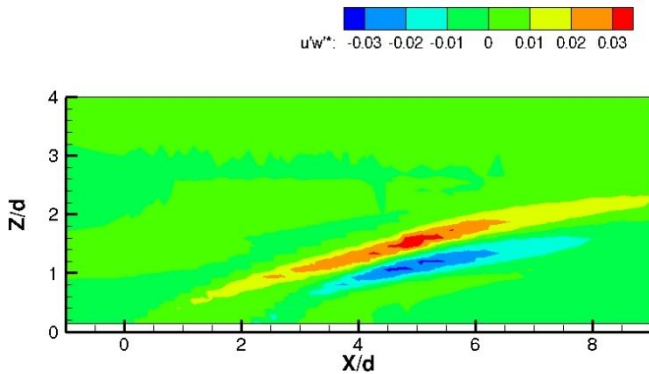


Fig 11. Turbulent stress $u'w'$ along coolant jet centerline at $BR \sim 2$

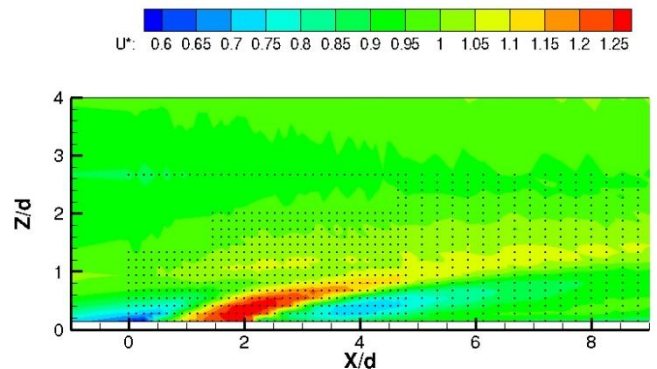


Fig 14. U-velocity along jet centerline at $BR \sim 1$

The streamwise plane in Figure 15 shows that the counter-rotating vortex pair appears closer to the wall than was the case for the high blowing ratio.

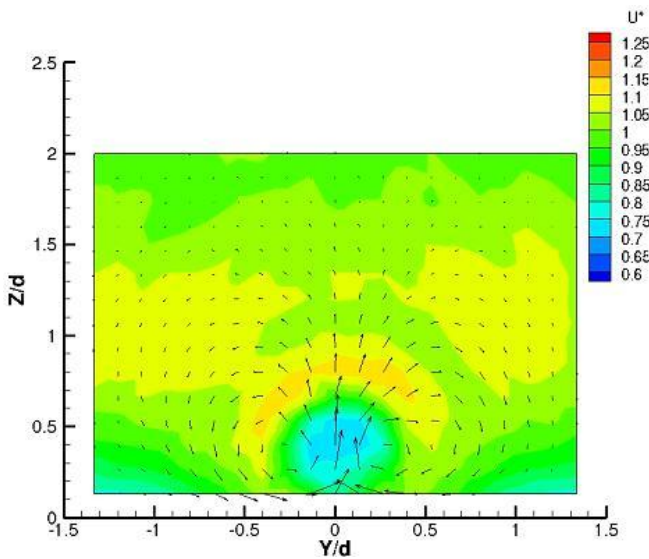


Fig 15. Vectors and U-velocity contours at $X/d \sim 4$ at $BR \sim 1$

The velocity fluctuations in all three directions (Figures 16 through 20) are lower than at the higher blowing ratio. The centerline contours (Figures 16 and 18) also suggest elevated fluctuations in the shear layers as was the case at high blowing ratio but more pronounced there.

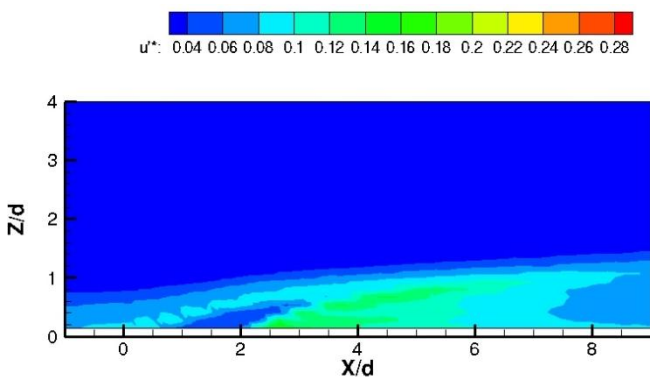


Fig 16. Turbulent fluctuations u' along jet centerline at $BR \sim 1$

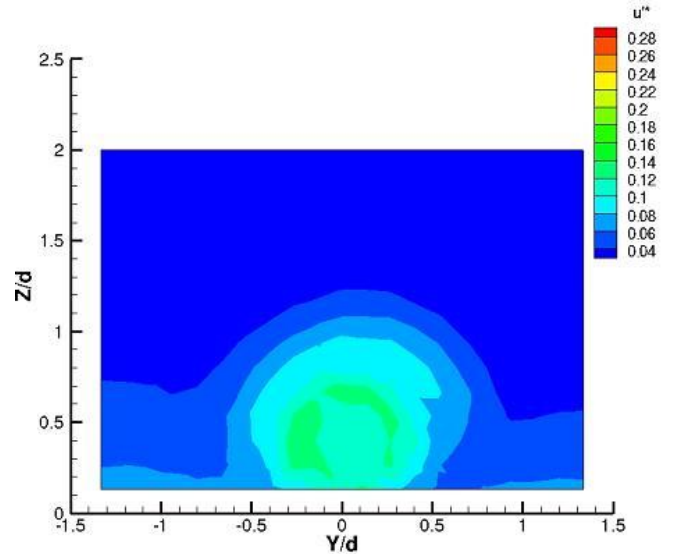


Fig 17. Turbulent fluctuations u' at $X/d \sim 4$ at $BR \sim 1$

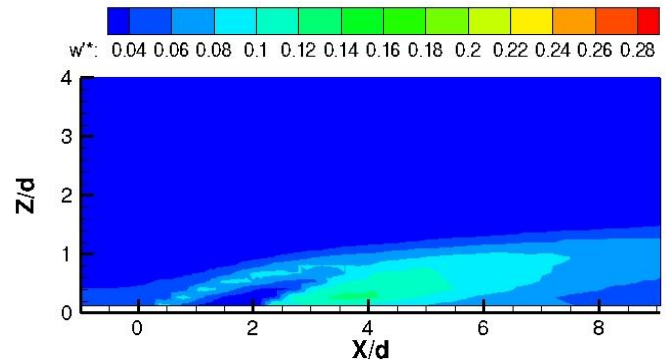


Fig 18. Turbulent fluctuations w' along jet centerline at $BR \sim 1$

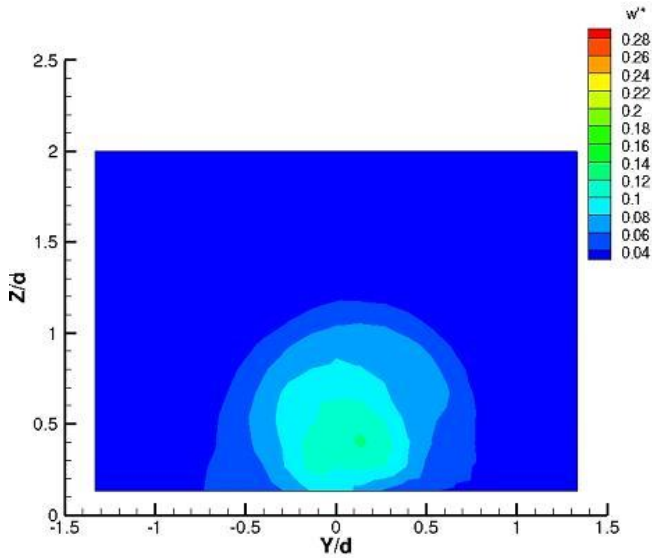


Fig 19. Turbulent fluctuations w' at $X/d \sim 4$ at $BR \sim 1$

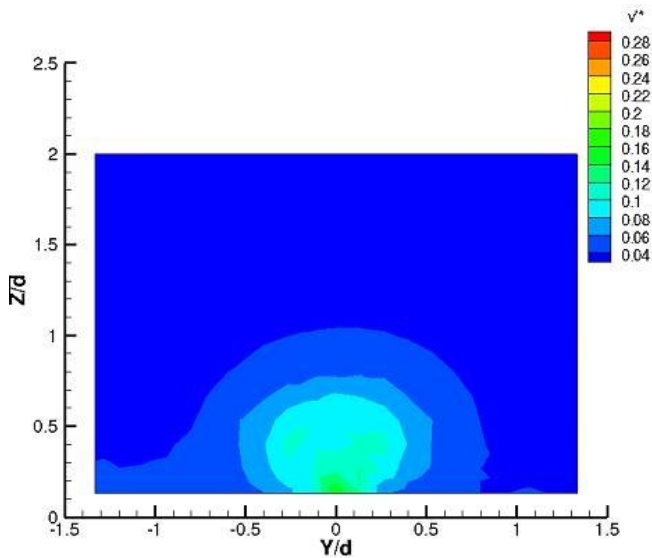


Fig 20. Turbulent fluctuations v' at $X/d \sim 4$ at $BR \sim 1$

Figures 21 and 22 show the normalized shear stress \overline{uw}/U_∞^2 along the jet centerline and at the streamwise location X/d of 4. As with the higher blowing ratio, there appears to be a negative and a positive direction to the stress and the highest intensity is along the shear layer, both the freestream side and the wake side of the jet. The magnitude however is significantly lower; it is at least one order of magnitude lower than the high blowing ratio case. Figure 22 does not show as strong a negative stress as the centerline data suggests should be at this location, which could be due to a probe misalignment. Figure 23 shows the normalized

\overline{uw}/U_∞^2 component of the turbulent shear stress. The magnitude of this component of stress is low and it appears to be somewhat symmetric, which is different than at the high blowing ratio (Figure 13).

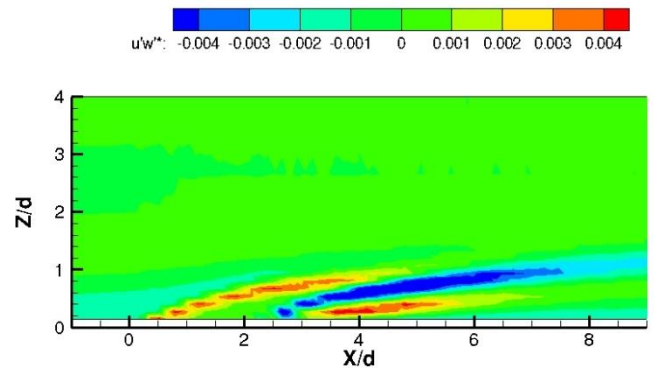


Fig 21. Turbulent stress $u'w'$ along jet centerline at $BR \sim 1$

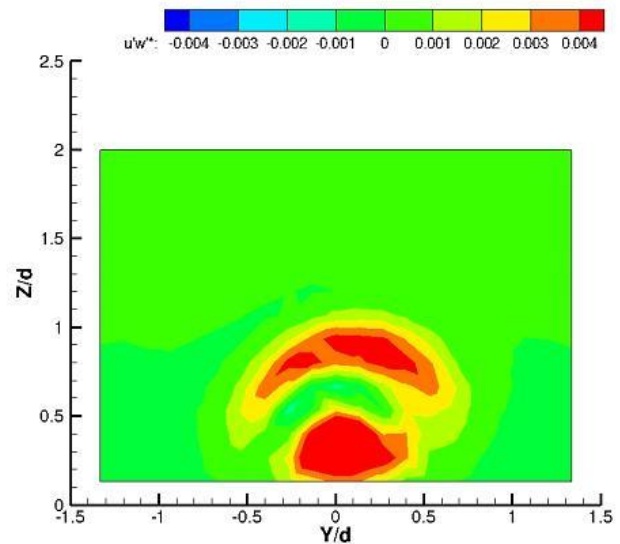


Fig 22. Turbulent stress $u'w'$ at $X/d \sim 4$ at $BR \sim 1$

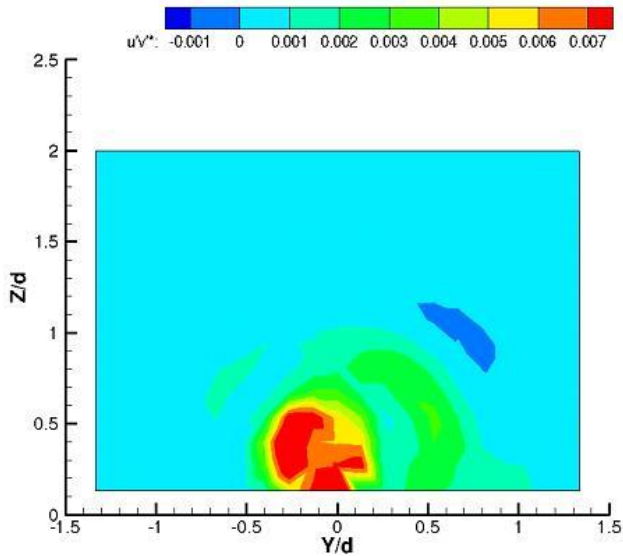


Fig 23. Turbulent stress $u'v'$ at $X/d \sim 4$ at $BR \sim 1$

COMPARISON WITH PRIOR ART

The authors are unaware of an identical data set to compare with directly. There are either differences in the geometry (injection angle, length of feed hole, etc) or differences in the flow conditions (blowing ratio, density ratio, velocity ratio, freestream turbulence, etc). However an attempt was made to make a comparison with data from [7] that is marginally similar to the test setup in the current study. This reference mainly reports results for a density ratio of 2 and measures vertical and streamwise components of velocity for a mass flux ratio of 0.5. The film hole is at 35 degrees and the L/D of the hole is 3.5 (i.e. a short hole). There is one data set presented at a density ratio of 1 for comparison, with blowing ratio of 0.5. Note that the present work has a mass flux ratio of 1 and 2 (which is higher than the highest case presented in [7]), the injection angle is 30 degrees and the L/D of the hole is 18.

Comparing Figure 24 (Figure 6a of [7]) for nearfield turbulence level at a density ratio of 1, mass flux ratio of 0.5 with Figure 16 shown earlier, we find that there are similarities. Pietrzyk shows intensities of up to 18% in the shear layer, which is similar to Figure 16. Furthermore, there appears to be two peaks in the turbulence level at the hole exit, one at the leading edge and one at the trailing edge of the hole indicative of the turbulence intensity due to shearing. These two peaks also appear in the current results in Figure 16. Note however that the Pietrzyk turbulence in Figure 24 is based on u and w fluctuations whereas Figure 16 in the current paper is based on u only.

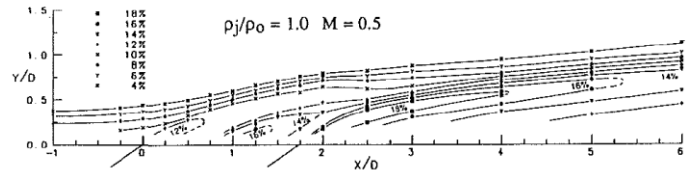


Fig 24. Nearfield turbulence levels (reproduced from Fig 6a of [7])

A second comparison can be made to Figure 25 (Figure 7a of [7]) for the nearfield turbulent shear stress that is plotted in Figure 21 of this paper. The shear stress is of a similar order of magnitude reaching -0.007 in both data sets. The current study however shows a larger range including more positive values of shear stress along with the negative values. The features at the hole leading edge and trailing edge are also present in both data sets.

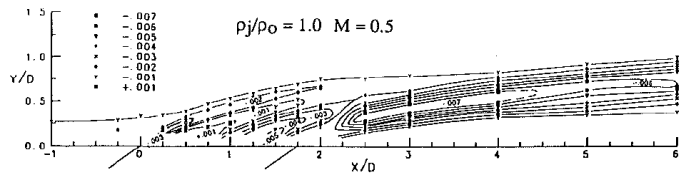


Fig 25. Nearfield turbulent shear stress (reproduced from Fig 7a of [7])

Therefore, the results from the current study are similar to prior art in magnitude for both the turbulent fluctuations and Reynolds stress as well as some of the features.

SUMMARY AND CONCLUSIONS

Hotwire anemometry is used to measure the velocity components and turbulence fluctuations and stresses in a large scale film cooling model at two nominal blowing ratios of 2 and 1. Experimental surveys are presented at the centerline of the jet and at streamwise locations. The velocity contours clearly show that the jet is lifted and the vectors and contour at the streamwise planes show the distinct kidney vortex that is often noted and attributed to the reduced effectiveness of the film as the vortex pair pushes the hot gas from the free stream down towards the wall. The jet is deflected more at the lower blowing ratio of 1 but the film is still not completely attached. Velocity fluctuations in the freestream direction are significant and can be up to 30% of the freestream velocity and are thus significant for the case of high blowing and about half that intensity for the low blowing. In the wall-normal direction, the fluctuations are also significant and locally in some regions exceed 25% of the freestream velocity. The fluctuations in the hole-to-hole direction are smaller at about 10% intensity for the high blowing ratio case and about half that for the lower blowing ratio. The highest turbulence stresses occur along the shear layer between the

jet and the freestream, both on the upstream interface and downstream wake layer. The normalized stresses \overline{uw}/U_∞^2 and \overline{vw}/U_∞^2 are at least one order of magnitude lower than the intensity of the velocity fluctuations and in the case of the \overline{uv}/U_∞^2 there appears to be asymmetry in the results but with the values being as small as they are this asymmetry is inconclusive. The detailed results are presented methodically and comprehensively with the goal of providing a test bank of data for CFD model development and validation.

ACKNOWLEDGMENTS

The research was carried out as part of the Subsonic Fixed Wing Project under NASA's Fundamental Aeronautics Program whose support is acknowledged. The authors would like to acknowledge the support of the NASA Glenn Faculty Fellowship program and the input of Dr. Khairul Zaman of NASA Glenn Research center on hotwire measurements.

REFERENCES

- [1] Goldstein, R.J., 1971, "Film Cooling," *Advancement in Heat Transfer*, Vol.7, pp. 321-379
- [2] Thole, K.A., Sinha, A.K., Bogard, D.G., and Crawford, M.E., 1990, "Mean Temperature Measurements of Jets in Crossflow for Gas Turbine Film Cooling Applications," *Third International Symposium on Transport Phenomena and Dynamics of Rotating Machinery*, Honolulu.
- [3] Sinha, A.K., Bogard, D.G., and Crawford, M.E., 1991, "Film-Cooling Effectiveness Downtream of a Single Row of Holes with Variable Density Ratio," *Journal of Turbomachinery*, Vol. 113, pp. 442-449.
- [4] Foster, N.W., and Lampard, D., 1980, "The flow and film cooling effectiveness following injection through a row of holes," *ASME Journal of Engineering for Power*, Vol. 102, pp. 584-588.
- [5] Kohli, A., and Bogard, D.G., 1997, "Adiabatic effectiveness, thermal fields, and velocity fields for film cooling with large angle injection," *Journal of Turbomachinery*, Vol. 119, pp. 352-358.
- [6] Foster, N.W., and Lampard, D., 1975, "Effect of density and velocity ratio of discrete hole film cooling," *AIAA Journal*, Vol. 113, pp. 1112-1114.
- [7] Pietrzyk, J.R., Bogard, D.G., and Crawford, M.E., 1990, "Effect of density ratio on the hydrodynamics of film cooling," *Journal of Turbomachinery*, Vol. 112, pp. 437-443.
- [8] Pietrzyk, J.R., Bogard, D.G., and Crawford, M.E., 1989, "Hydrodynamic measurements of jets in crossflow for gas turbine film cooling application," *Journal of Turbomachinery*, Vol. 111, pp. 139-145.
- [9] Pietrzyk, J.R., 1989, "Experimental study of interaction of dense jets with a crossflow for gas turbine applications," PhD thesis, University of Texas at Austin.
- [10] Walters, D.K., and Leylek, J.H., 1997, "A systematic computational methodology applied to a three-dimensional film-cooling flowfield," *Journal of Turbomachinery*, Vol. 119, pp. 777-785.
- [11] El-Gabry, L., Heidmann, J., and Ameri, A., 2010, "Penetration characteristics of film-cooling jets at high blowing ratio," *AIAA Journal*, Vol. 48, pp. 1020-1024.
- [12] Andreopoulos, J. and Rodi, W., 1984, "Experimental investigations of jets in a crossflow," *Journal of Fluid Mechanics*, Vol. 138, pp. 93-127.
- [13] Kohli, A., and Bogard, D.G., 2005, "Turbulent transport in film cooling flows," *Journal of Heat Transfer*, Vol. 127, pp. 513-520.
- [14] Thurman, D., E-Gabry, L., Poinsatte, P., Heidmann, J., 2011, "Turbulence and Heat Transfer Measurements in an Inclined Large Scale Film Cooling Array – Part II, Temperature and Heat Transfer Measurements," ASME paper GT2011-46498, *ASME Turbo Expo 2011*, Vancouver.
- [15] Yavuzkurt, S., 1984, "A Guide to Uncertainty Analysis of Hot-Wire Data," *Journal of Fluids Engineering*, Vol. 106, pp. 181-186.
- [16] Bruun, H.H., 1995, "Hot-wire Anemometry: Principles and Signal Analysis," Oxford University Press.